RESEARCH ARTICLE

Machine learning-based estimation of respiratory fluctuations in a healthy adult population using resting state BOLD fMRI and head motion parameters

Abdoljalil Addeh[1,2,3,4] | **Fernando Vega**[1,2,3,4] | **Amin Morshedi**[1,2,3,4] | **Rebecca J. Williams**[5] | **G. Bruce Pike**[3,4,6] | **M. Ethan MacDonald**[1,2,3,4]

[1]Department of Biomedical Engineering, Schulich School of Engineering, University of Calgary, Calgary, Alberta, Canada

[2]Department of Electrical & Software Engineering, Schulich School of Engineering, University of Calgary, Calgary, Alberta, Canada

[3]Department of Radiology, Cumming School of Medicine, University of Calgary, Calgary, Alberta, Canada

[4]Hotchkiss Brain Institute, Cumming School of Medicine, University of Calgary, Calgary, Alberta, Canada

[5]Faculty of Health, Charles Darwin University, Casuarina, Australia

[6]Department of Clinical Neurosciences, Cumming School of Medicine, University of Calgary, Calgary, Alberta, Canada

Correspondence
M. Ethan MacDonald, Department of Biomedical Engineering, Schulich School of Engineering, University of Calgary, ICT 452, Schulich School of Engineering, 2500 University Dr NW, Calgary, AB, Canada.
Email: ethan.macdonald@ucalgary.ca

Abstract

Purpose: External physiological monitoring is the primary approach to measure and remove effects of low-frequency respiratory variation from BOLD-fMRI signals. However, the acquisition of clean external respiratory data during fMRI is not always possible, so recent research has proposed using machine learning to directly estimate respiratory variation (RV), potentially obviating the need for external monitoring. In this study, we propose an extended method for reconstructing RV waveforms directly from resting state BOLD-fMRI data in healthy adult participants with the inclusion of both BOLD signals and derived head motion parameters.

Methods: In the proposed method, 1D convolutional neural networks (1D-CNNs) used BOLD signals and head motion parameters to reconstruct the RV waveform for the whole fMRI scan time. Resting-state fMRI data and associated respiratory records from the Human Connectome Project in Young Adults (HCP-YA) dataset are used to train and test the proposed method.

Results: Compared to using only BOLD-fMRI data for a CNN input, this approach yielded improvements of 14% in mean absolute error, 24% in mean square error, 14% in correlation, and 12% in dynamic time warping. When tested on independent datasets, the method demonstrated generalizability, even in data with different TRs and physiological conditions.

Conclusion: This study shows that the respiratory variations could be reconstructed from BOLD-fMRI data in the young adult population, and its accuracy could be improved using supportive data such as head motion parameters. The method also performed well on independent datasets with different experimental conditions.

KEYWORDS
BOLD fMRI, convolutional neural network, HCP-YA, head pseudomotion, physiological correction, respiratory variation

1 | INTRODUCTION

fMRI is a powerful neuroimaging technique that has revolutionized the way the brain is studied. However, the BOLD signal measured by fMRI is influenced not only by neuronal activity and its associated cerebral blood flow (CBF) and oxygen metabolism ($CMRO_2$) effects, but also by the effects of non-neural contributors such as low-frequency respiratory variation.[1–5] Low-frequency respiratory confounds can reduce the SNR of fMRI data, making it more difficult to detect small changes in brain activity, resulting in reduced sensitivity and statistical power in fMRI studies.[6]

Recently, several model-based approaches have been developed to remove the effect of low-frequency physiological variations from fMRI signals.[1,7–9] In model-based methods, the related BOLD components are modeled as the convolution of a respiratory measure (extracted from a respiratory signal recorded during the fMRI scan) and the hemodynamic response function.[10,11] Respiratory data are not routinely recorded in many fMRI experiments due to the lack of measurement equipment in the imaging suite, insufficient time to set them up, subject compliance, or financial issues. Even in the fMRI studies where respiratory data are collected, a significant proportion of the data is corrupted and unusable. As an example, up to 87% of the respiratory signals in the Human Connectome Project in Development (HCP-D) are not usable.[12] Similarly, in the HCP in Young Adults (HCP-YA) dataset, around 51% of respiratory data is deemed unusable.[13] This limitation hinders the effective removal of confounding signals caused by respiratory variations.

Several machine learning-based approaches have been developed recently that utilize the information contained within BOLD signals to estimate respiratory variation (RV) waveforms.[14–16] These methodologies were rigorously evaluated on the HCP-YA dataset, with promising results. However, the following specific constraints were identified during their deployment. First, the BOLD signals were subjected to band-pass filtering within a narrow frequency range of 0.01–0.15 Hz and were temporally downsampled by a factor of 2. The band-pass filtering could potentially disregard vital physiological information existing at frequencies beyond the filtering range, especially since respiratory-induced BOLD fluctuations are known to be contained in higher frequencies.[10,17] Furthermore, the downsampling process reduces the temporal resolution, risking the loss of critical transient respiratory events, which are essential for precise RV waveform estimation. Additionally, the consideration that the optimal frequency threshold for filtering may vary among individuals poses a further challenge to the standardization of this approach across diverse populations. Second, the

RV signals underwent the same filtering and downsampling protocol. Yet, the RV signals in the HCP-YA dataset have a substantial component within the (0.2–0.4) Hz frequency band.

Head motion represents another technical obstacle in fMRI, but it has been shown that the estimated head motion parameters derived from retrospective image realignment algorithms work well for correcting bulk motion.[18,19] However, head motion parameters can also give informative information about the subject's respiratory activity. It has long been recognized that respiration perturbs the magnetic field (B_0),[20] and multiband imaging (simultaneous multi-slice sequences [SMS]) might have intensified perturbations.[18] Recent studies have shown that respiration generates real head motion,[13,21,22] and pseudomotion of the head,[13,18,19] at the respiratory rate (~0.3 Hz for healthy adults), and a very low-frequency real and pseudomotion during and after deep breaths (~0.12 Hz).[13] Understanding the complex relationship between head motion and respiration within the magnetic resonance environment is challenging due to numerous influencing factors. These dynamics are not easily captured by conventional analytical approaches or straightforward predictive algorithms. Consequently, there is a need for advanced deep learning architectures that have the potential to uncover the subtle, non-linear correlations that traditional methods may overlook. Head motion parameters during an fMRI scan thus contain valuable information regarding the different respiratory events and main breathing rate, which can help the machine learning algorithm estimate the RV waveform. As an example, the work of Fair et al.[18] and Kaplan et al.[19] illustrates that estimated head motion parameters may reflect the breathing rate. To accommodate individual differences in breathing patterns, the investigators tailored the cutoff frequency of the notch filter, aiming to eliminate respiratory-induced head motion in their studies. Consequently, leveraging head motion parameters with machine learning methodologies might offer a promising avenue for improving RV estimation.

To address previously identified gaps, we previously introduced a strategy by harnessing the capabilities of three convolutional neural networks (CNNs) for the reconstruction of the RV signal throughout the entirety of fMRI scan durations.[12] This approach deliberately eschews band-pass filtering of BOLD and RV signals, ensuring the complete spectrum of physiological data is retained and utilized by our machine learning framework. This methodology represents a significant advancement in the utilization of machine learning techniques, aiming to both refine the precision of RV signal predictions derived from BOLD signals and broaden the temporal scope of the reconstructed RV signal. However, the incorporation of head

motion parameters may further improve the performance of RV reconstruction.

The current work asks the question if the inclusion of head motion parameters can improve machine learning models for estimating RV from resting state BOLD signals. We expect that the inclusion of head motion parameters will result in at least a 5% improvement in our measurement criteria, which include mean absolute error (MAE), mean square error (MSE), correlation, and dynamic time warping (DTW). In this study, we propose a 1D-CNN that uses both BOLD signals and head motion parameters extracted from the fMRI images to reconstruct the RV waveform. The Supporting Information provide additional detail regarding the impact of respiration on BOLD signals and estimated head motion parameters.

2 | METHODS

2.1 | Dataset and preprocessing

In our study, the primary data utilized for training and testing were derived from the HCP-YA dataset.[23] Validation was subsequently performed on two additional independent datasets, referred to herein as Dataset 1 and Dataset 2.[24,25] Detailed information regarding the datasets, quality control of respiration traces, and the fMRI data preprocessing pipeline can be found in Supporting Information File, Section 1.

2.2 | Proposed method

In this paper, we introduce a novel technique for the reconstruction of RV waveforms using BOLD signals combined with head motion parameters. The foundation for this approach is based on five pivotal assumptions:

> **Assumption 1.** Fluctuations in breathing depth and rate at low frequencies influence the BOLD signal. For instance, a deep inhalation results in a decline in the BOLD signal, while breath-holding elevates it, as depicted in Figure S.1. Consequently, BOLD signals offer significant insights into respiratory patterns.

> **Assumption 2.** Fluctuations in CO_2 levels due to respiratory changes instigate chemoreflexes that modify the subsequent breathing depth and rate.[26,27] This results in a feedback loop with a chemoreflex-mediated cycle observed to last approximately 25 s or longer. Current BOLD signals influenced by

respiratory changes are therefore not just a consequence of present breaths but also carry information about prior respiratory events. Machine learning models are capable of capturing and utilizing historical BOLD signal data to reconstruct the current RV timeseries.

> **Assumption 3.** Involuntary head motions, triggered by actions like nodding during respiratory cycles, yawning, sneezing, and other factors, manifest in the calculated head motion parameters at respiration frequency. This implies that these head motion parameters can be a valuable source of information regarding various respiratory events and their associated frequencies.

> **Assumptions 4.** Respirations contaminate estimated head motion parameters by generating apparent pseudomotion at the frequency of the breathing rate. Hence, the derived head motion parameters can be an instrumental source in determining both breathing rate and depth.

> **Assumptions 5.** Actual head motion and pseudomotion may appear in any motion parameters. So, estimated head motion parameters in all directions contain information about breathing.

The proposed technique integrates three 1D-CNNs functioning in the temporal domain of both the BOLD time series and head motion parameters. This utilization of CNNs stems from their innate capability to discern patterns that remain invariant regardless of their position or translation. A schematic of the input–output relationship in the methodology is presented in Figure 1. For computational efficiency and to boost the SNR of the input signals, the mean BOLD signal time series from 90 functional regions of interest (ROIs)[28] is utilized as the primary model input.

The model input is formulated using a sliding time-window approach. Specifically, fMRI-ROI signals are fragmented into brief, overlapping time-windows of 65 TRs, as delineated in Figure 1. For each time window, the model outputs a single time-point estimate of the RV signal at the first point of the window (Method 1 in Figure 1), middle point of the window (Method 2 in Figure 1), and end point of the window (Method 3 in Figure 1). The RV is defined as the SD of the respiratory waveform within a 6-s sliding window centered at each time point.[4] In Method 2, the CNN can use both past and future information, but in Method 1 and 3 it can only use the future and past information, respectively.
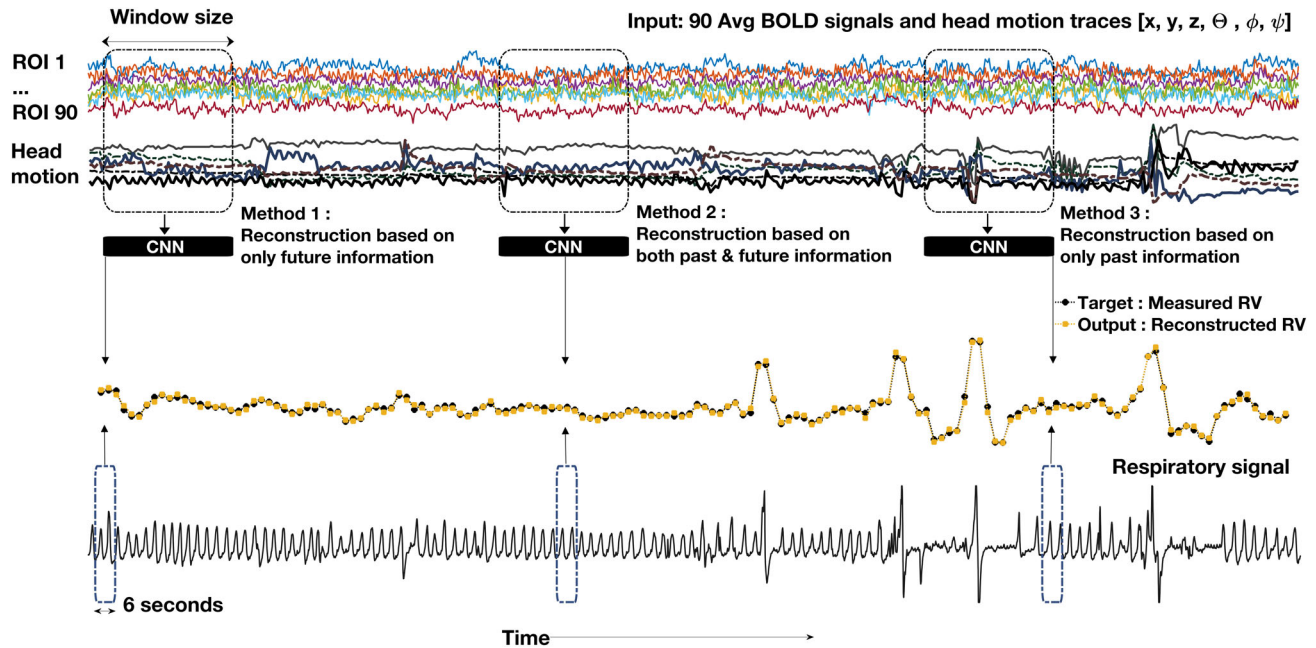
FIGURE 1 Schematic representation of the proposed method for reconstructing RV waveforms from BOLD signals and head motion parameters. The input consists of the average BOLD signals from 90 ROIs and six head motion parameters. The model employs three different CNN-based approaches: Method 1 uses only future BOLD signals and estimates RV for the initial volumes (from TR 5 to TR 36), Method 2 integrates both past and future BOLD signals and estimates RV for the central volumes (from TR 37 to TR 1163), and Method 3 relies exclusively on past BOLD signals and estimates RV for the final volumes (from TR 1164 to TR 1196). The RV estimation begins at TR 5 and ends at TR 1196 to ensure sufficient data within the 6-s window required for accurate computation. The window size, set to 65 TRs, determines the segment of data processed by the CNN. The outputs of these methods are combined to reconstruct the complete RV waveform, with performance improvements observed when head motion parameters are included alongside BOLD signals.

The size of the moving window is selected as 65 in the proposed method. For Method 2 as an example, BOLD signals and head motion parameters centered at each RV point covering 32 TRs before and after were used as the input. Therefore, each input had a size of $[65 \times 96]$, where 65 is the window size, and 96 is the number of ROIs and six head motion parameters. Due to this windowing procedure, the reconstructed RV signal in Method 2 yields only 1136 timepoints out of an original 1200. To circumvent this limitation and retain the crucial initial and final 32 timepoints, Methods 1 and 3 are employed. Collectively, these methods enable a complete RV reconstruction for the entire scan duration. Further details concerning the architecture of the proposed 1D-CNN model are provided in the Supporting Information, under Section 2.

2.3 | MODEL TRAINING

From 3946 resting-state fMRI scans across 1040 subjects in HCP-YA dataset, 945 scans from 468 were selected for the training and testing phases of the proposed methodology due to the viability of their respiratory data post spike-elimination and motion threshold (see Supporting Information, Section 3). The MSE was employed as the loss function during the model training, due to its effectiveness in penalizing larger prediction errors, which is crucial for high-precision reconstruction of respiratory variation from fMRI data.

To evaluate our model, we employed a 10-fold cross-validation methodology, consistent with standard practices.[29,30] The input–output dataset was divided into 10 subsets. For each cross-validation fold, nine subsets were used for training the model, while the remaining subset was designated for testing. This process was repeated 10 times, each time with a different subset as the test set, ensuring that each subset was utilized exactly once for testing. Additionally, 20% of the data within the training segment was allocated to validation in each fold. Each model was trained for 300 epochs per fold. This systematic rotation of subsets across folds ensures robust model evaluation by maintaining independent training and testing subsets across all iterations, minimizing potential biases.

Performance metrics from all iterations were compiled, and results were reported as the "average $\pm$ standard error (SE)" to provide a clear indication of the model's overall efficacy.[30] To effectively demonstrate the method's performance, violin plots were used illustrating the model's

performance over the unseen test data throughout the 10-fold cross-validation process. Additional technical details are provided in Supporting Information, Section 4, and model performance evaluation in Section 5.

3 | RESULTS

3.1 | Relationship of respiration, head motion, and BOLD signal

The analysis revealed contributions of respiratory-induced true motion, respiratory-induced head pseudomotion, and random head motion to the observed variability in the BOLD signal,[13,18,19] with each type of motion distinctly influencing the signal in different ways. Figure 2 shows the frequency content of the head motion parameters calculated using power spectral density estimation (MATLAB pmtm function). The respiration creates real- and pseudomotion of the head, especially in the phase-encoding direction, at a frequency of ~0.29 Hz (shown by red arrow), which is consistent with the normal breathing rate of young adults (~17 breaths per minute). It is typical for subjects to experience variations in their breathing rates during an fMRI scan. Such fluctuations can manifest across

various frequencies, leading to a broadening of the spectral peak. When deep breaths occur, the full process of inspiration and exhalation transpires more slowly than tidal breaths, evidently occupying about 8 s per cycle (approximately 0.12 Hz), in contrast to the main tidal rate of about 0.29 Hz.[13] These deep breaths represent infrequent, aperiodic low-frequency events that, while occurring at 0.12 Hz (shown by blue array).

Figure 3A presents a scatter plot of the primary respiratory frequency against the primary frequency of estimated head motion in the x-direction from 945 selected fMRI scans in HCP-YA dataset. The plots for the full signal and four segmented intervals demonstrate a substantial linear correlation, as evidenced by data points densely aggregated along the trend line, with respiration frequencies averaging at 0.302 ± 0.051 Hz and head motion frequencies at 0.298 ± 0.056 Hz. A notably high correlation of 0.95 (with a two-tailed significance level of <0.001) underscores a potent linear association between respiration and head motion. This relationship extends to other motion parameters, including the y-axis, z-axis, roll, yaw, and pitch directions. Figure 4B complements this by showing a line graph of the peak breathing rate variability across scans, illustrating occasional deviations beyond 0.2 Hz, yet maintaining a clear congruence with head motion frequencies. These
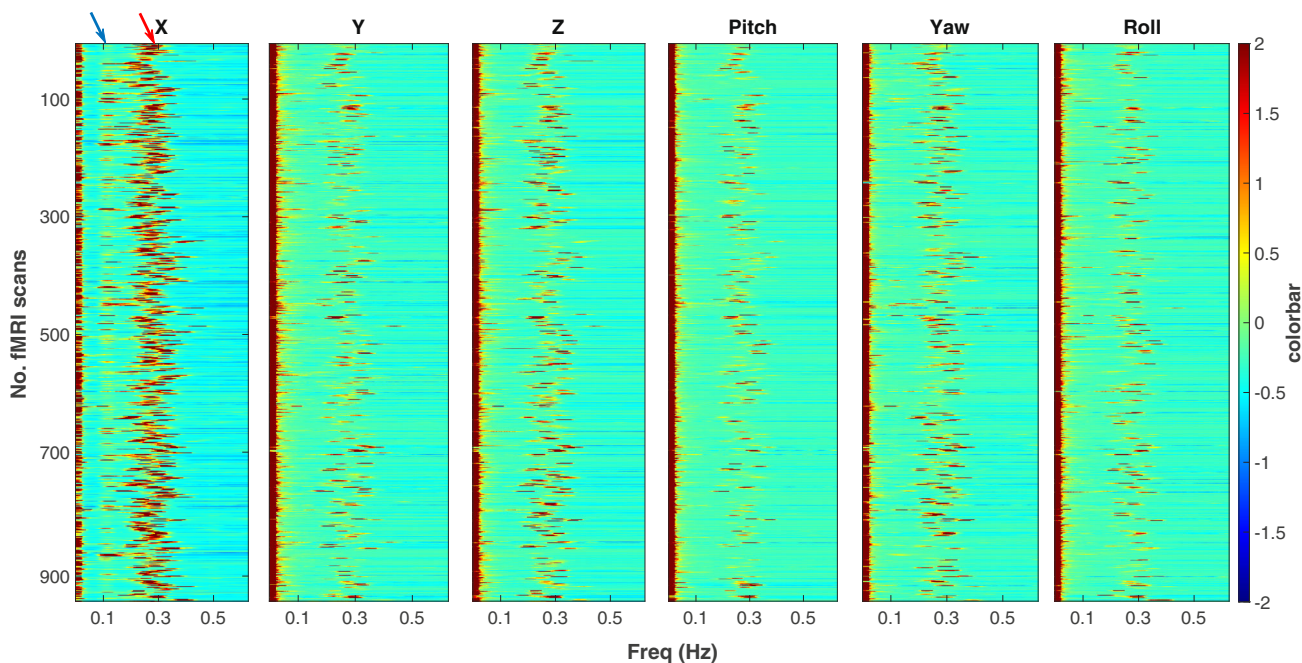

FIGURE 2 Power spectral density (PSD) analysis of head motion parameters across 945 fMRI scans from the HCP-YA dataset. The figure displays the frequency content of motion parameters (X, Y, Z translations, and pitch, yaw, roll rotations) with the color bar indicating the power intensity. The X-axis shows the frequency range from 0 to 0.625 Hz, and the Y-axis represents the fMRI scan number. The red arrow on the X-axis highlights the primary respiratory frequency (~0.29 Hz), which corresponds to the typical breathing rate in young adults. The blue arrow indicates the frequency of deep breaths (~0.12 Hz). Respiratory-induced head pseudomotion is most pronounced in the X-direction (phase-encoding direction in HCP-YA scans), as shown by the denser regions around 0.29 Hz, demonstrating the significant impact of respiration on head motion, especially in the phase-encoding direction.
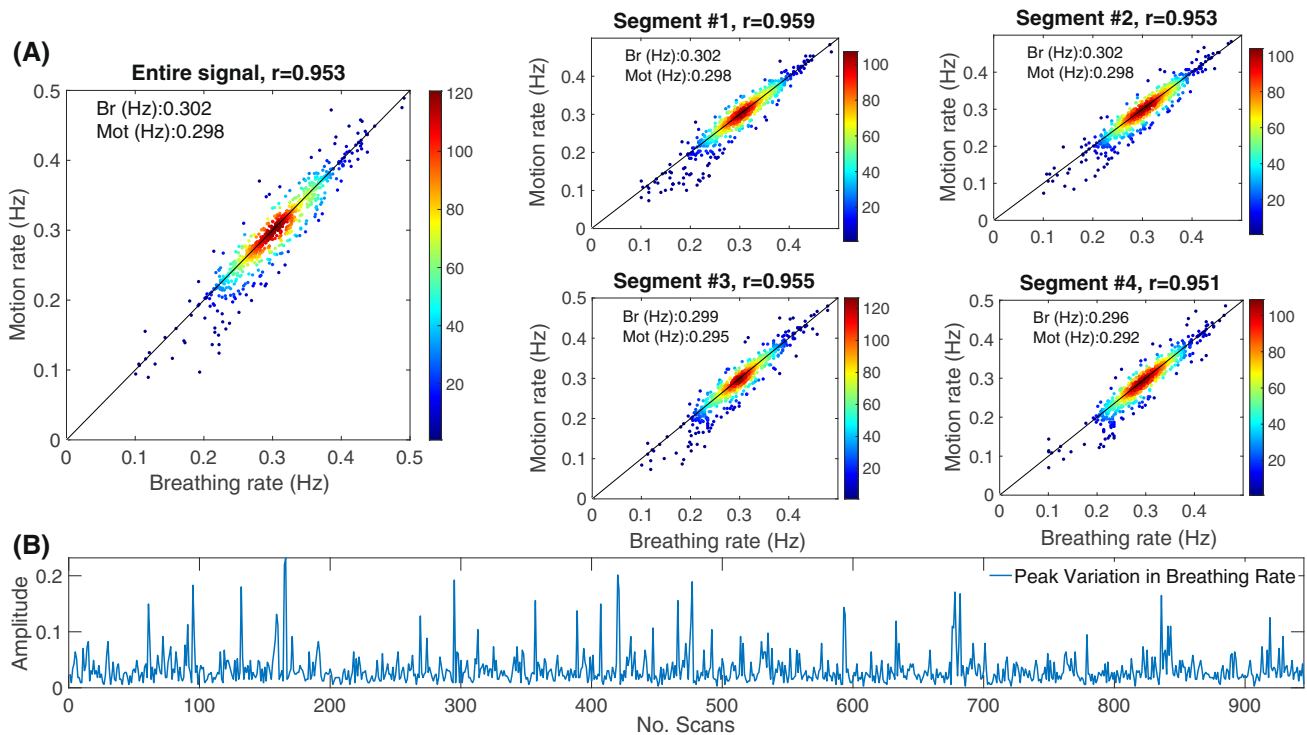
FIGURE 3 (A) Scatter plots illustrating the correlation between breathing rate and estimated head motion rate across the entire signal and four segmented intervals from 945 selected fMRI scans. The leftmost plot represents the entire signal, showing a strong positive correlation ($r = 0.953$) between breathing rate and head motion rate. The four segmented plots represent different sections of the fMRI scan, with consistently high correlations (ranging from 0.951 to 0.959). The average breathing rate and motion rate are annotated within each plot. (B) A line graph depicting peak variations in breathing rate across all 945 scans, with the X-axis showing the scan number and the Y-axis representing amplitude. The graph highlights the variability in breathing rates during scan time, with occasional peaks exceeding 0.2 Hz. These findings suggest that head motion parameters are reliable indicators of breathing rate in fMRI data, supporting the use of head motion as a non-invasive proxy for respiratory monitoring.

findings support the efficacy of using head motion parameters as robust proxies for respiratory rate monitoring in fMRI environments. Intriguingly, high RV variability is not limited to prominent respiratory events. Our analysis of the HCP-YA dataset reveals that RV also increases when subjects breathe slowly at a consistent amplitude, compared to when they breathe rapidly with the same amplitude. This observation conforms to the definition of RV as the SD of the respiratory waveform within a 6-s sliding window centered at each time point. We observed a significant negative correlation between the rate of head motion and RV variance ($r = -0.32$, p-value <0.001), as shown in Figure S.3. This relationship is further enriched by a strong positive correlation between breathing rate and head motion rate, suggesting that head motion parameters provide critical insights into the amplitude of RV in scenarios where the subject's breathing rate is slow but consistent. These insights may not be as readily detectable from BOLD signals alone.

Figure 4 displays three respiratory and motion parameters on the x-axis. It is evident that respiratory signals and motion parameters vary in tandem. For instance, in

Figure 5A,B, a decrease in the subject's breathing rate corresponds to a more gradual variation in the head motion parameter, as highlighted by the red arrows. Similarly, in Figure 5C, a deep inhalation by the subject aligns with this slower head motion variation. In addition, Figure 5 illustrates that during pronounced respiratory events, such as deep breaths, there is a significant alteration in the amplitude of head motion parameters. To account for this, we normalized both respiratory and motion parameters and then calculated the SD for each signal. Our analysis unveiled a modest positive correlation of 0.17 between the SDs of the respiratory and head motion signals ($p < 0.001$, 2-tailed). Additionally, Power et al.[13] demonstrated a significant association between increased RV variability and increased head motion ($r = 0.57$, $p < 0.001$), reinforcing the value of head motion parameters as reliable indicators of both respiratory rate and depth, as well as RV variation.

In addition to respiratory-induced head motions, random head motions that are not related to respiration can also occur. These random head motions, being true motions, generate BOLD signal artifacts primarily through spin history effects. Figure 5 shows an example of random
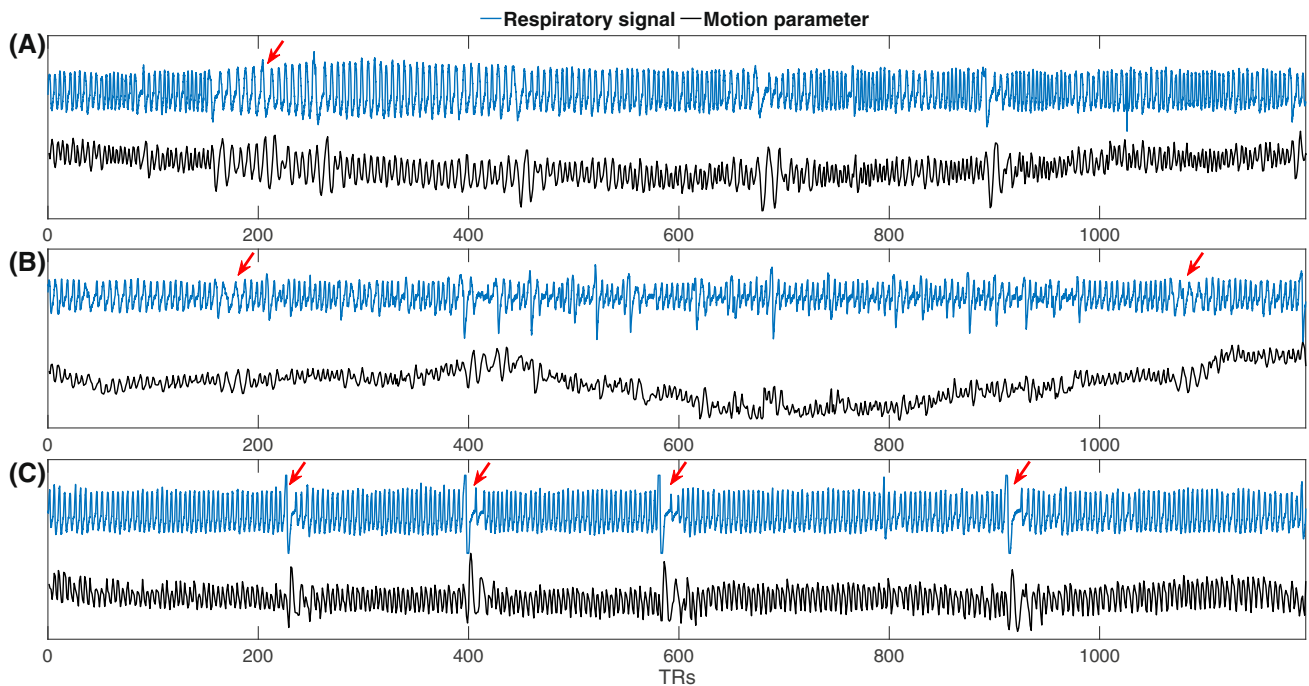
FIGURE 4 Comparison of respiratory signals (blue) and head motion parameters (black) for three different fMRI scans from the HCP-YA dataset. (A-C) Each represent a full scan, illustrating how respiratory fluctuations correspond with head motion changes over time. Red arrows indicate instances where significant changes in the respiratory signal align with noticeable shifts in head motion, suggesting a close relationship between the two. This alignment highlights the potential of using head motion parameters as proxies for respiratory variation in fMRI analyses.
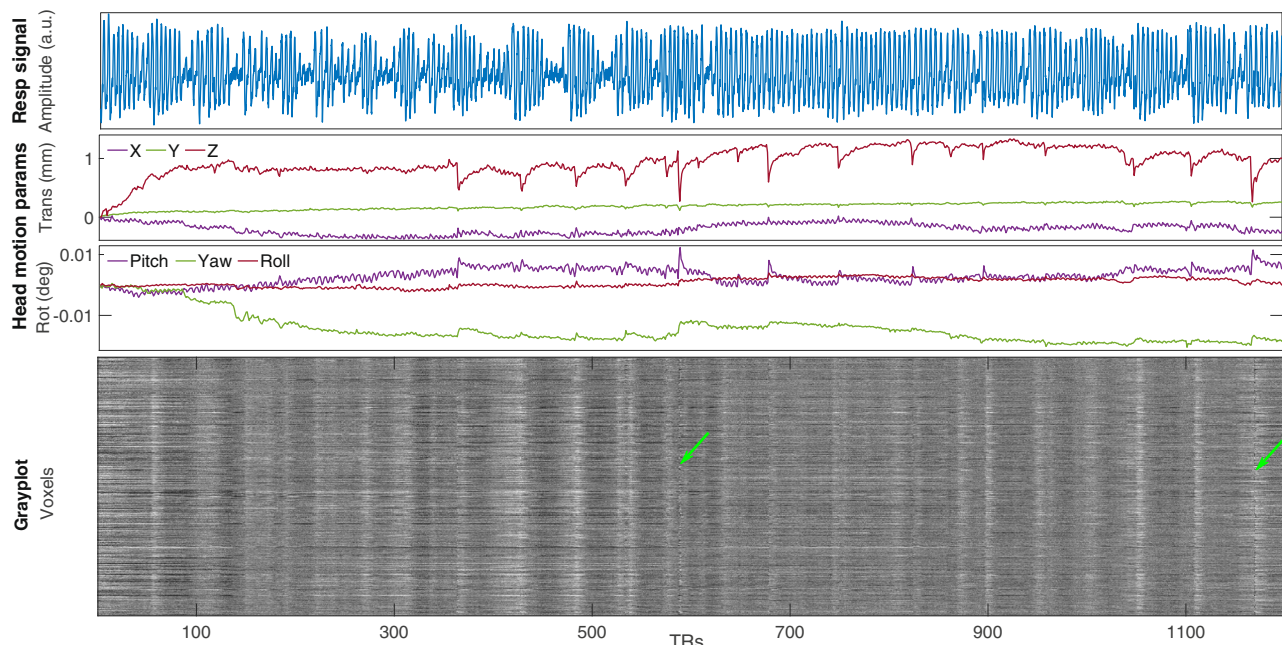

FIGURE 5 Comparison of respiratory signals (blue) with head motion parameters (X, Y, Z translations, and pitch, yaw, roll rotations) over the full duration of an fMRI scan from the HCP-YA dataset. The top panel illustrates the amplitude of the respiratory signal, while the middle panels display the six head motion parameters, reflecting translational and rotational movements. The bottom panel presents a grayplot depicting the temporal dynamics of the BOLD signal across voxels. Green arrows highlight instances where random head motion (indicated by vertical black bands), distinct from respiration-induced head motion, impacts the BOLD signal. The variation in the BOLD signal caused by random head motion shows a significant difference compared to the BOLD signal variation due to respiratory fluctuations, as demonstrated in Figure S.3 in the Supporting Information. These visualizations emphasize the differential effects of random head motion on BOLD signal fluctuations, distinguishing them from the influence of respiratory variations.

head motion and its impact on BOLD signal using grayplots. Grayplots visualize fMRI signal dynamics by mapping temporal sequences and spatial voxel distributions, aiding in artifact identification and data quality assessment.[31] The BOLD signal variation generated by a random true head motion (vertical black band indicated by green arrow) has a significant difference with BOLD signal variation because of respiratory variation shown in Figure S.4 in the Supporting Information. This distinction between the effects of true head motion and respiratory variation on BOLD signals is critical. The CNN model can exploit these differences by utilizing all available information—both BOLD signals and head motion parameters—as inputs to learn and distinguish between random head motion and respiratory-induced head motion. By effectively identifying and differentiating the BOLD signal variations caused by these two types of motions, the model can filter out confounding signals, thereby improving the accuracy of RV estimation. This comprehensive approach allows for a more precise reconstruction of the RV waveform from the combined BOLD signals and head motion parameters.

The emphasis on head motion along the X-axis in Figures 3–5 is particularly relevant because, in HCP-YA scans, the phase encoding direction is left-right, corresponding to the X-axis. Respiratory-induced pseudo-motion is most prominent in this direction due to B_0 magnetic field perturbations caused by chest movement during breathing. However, it is important to note that respiratory-related head motion is not limited to the X-axis. While the X-axis shows prominent factitious motion, other directions, such as the Y-axis (anterior–posterior) and Z-axis (superior–inferior), also exhibit both real and apparent respiratory-induced head motion. These motions result from true brain movement transmitted through mechanical linkage via the neck, as well as potential leakage of the B_0 artifact into other directions.[13,18] Consequently, respiratory artifacts can influence all three axes, though they are most pronounced in the phase encoding direction, which typically aligns with the X-axis in HCP-YA scans. This focus on the X-axis in our analysis reflects its importance in assessing respiratory effects on fMRI data.

3.2 | MODEL PERFORMANCE

In this section, each reported value or plot represents results over the unseen test data in 10-fold cross-validation in terms of MAE, MSE, r, and DTW. In these experiments, a window size of 65 was employed. The influence of window size on the model's performance is explored in the Supporting Information, Figure S.5. Figure 6 highlights

the superiority of the current method over the preceding model by Salas et al.,[16] which exclusively incorporated BOLD signals for machine learning inputs. The inclusion of head motion parameters significantly enhances the reconstruction accuracy of RV, which is evident during significant respiratory events (marked by orange arrows) as well as during periods of minimal breathing variability (indicated by green arrows). The CNN leverages the additional head motion data alongside BOLD signals to infer respiratory rate and depth with improved precision. Despite this improvement, there remains no uniform pattern in pinpointing the most precise signal estimation across the various evaluation metrics. As illustrated in Figure 7, while Pearson correlation values suggest a more precise estimation for signal 'a', the MAE and MSE point to signal 'd' as being superior.

Figure 7 shows the performance of the CNN in terms of MAE, MSE, r, and DTW. For all metrics, using head motion parameters has improved the model's performance. The statistical analyses using Friedman test showed that there is a statistically significant difference between the three approaches (p-value <0.01). The accuracy of the reconstructed RV in the frequency domain is examined in the Supporting Information, Figure S.6.

The performance of the proposed model is compared with the model developed by Salas et al.,[16] in Table 1. In the five-layer CNN model developed by Salas et al., the number of filters in different layers are 20, 40, 80, 160, and 320, respectively, and ReLU is used in the hidden layers. This implementation is compared against the proposed model. In this comparison, BOLD signal and head motion parameters are used as the input of both CNN models. To summarize, the proposed method outperforms Salas's model with a significant difference in their performance (p-value <0.01) which shows the importance of the model's architecture and hyper-parameters. Further analysis on the impact of the model's hyper-parameters contributing to this performance difference is provided in Supporting Information File, Section 10, while Section 11 discusses additional strategies used to overcome limitations of previous methods.

An interesting application of the proposed method is reconstruction of the RV time course for scans without respiratory data or scans with poor quality respiratory data. The performance of the developed method is tested on a scan that respiratory data were not recorded. Due to the lack of a measured respiratory signal, it is not possible to evaluate the accuracy of the reconstructed RV signal in Figure 8. Heat maps and the subject's head motion parameters still provide insight. According to the vertical bands on the heat maps and the head motion parameters, there is a reasonable degree of accuracy in the RV estimation.
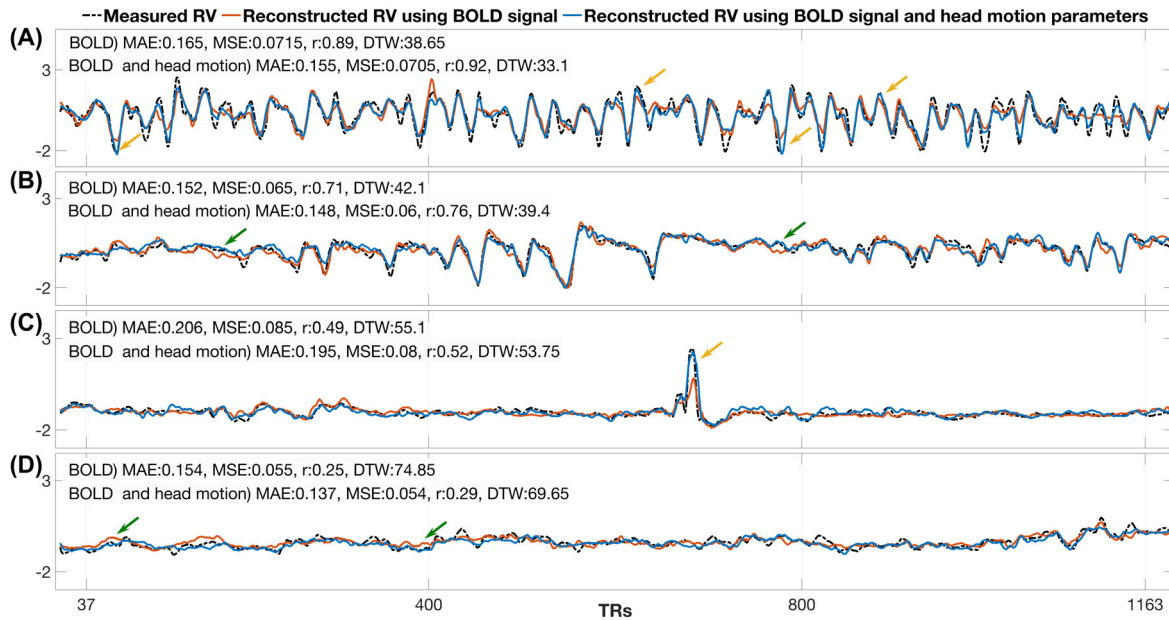
FIGURE 6 Comparison of reconstructed RV waveforms using BOLD signals alone and BOLD signals combined with head motion parameters across four entire fMRI scans from the HCP-YA dataset. (A-D) The measured RV (black dashed line) is compared with the reconstructed RV using only BOLD signals (red line) and the reconstructed RV using both BOLD signals and head motion parameters (blue line). Performance metrics are reported for each reconstruction method. Yellow arrows highlight instances where using head motion parameters improves the alignment between the reconstructed and measured RV during prominent respiratory pattern changes. Green arrows indicate areas where the reconstruction using both BOLD and head motion parameters provides a more accurate representation of the measured RV compared to using BOLD signals alone, particularly when the RV value is small. Estimating RV when it is small is challenging because subtle respiratory events may not significantly alter the BOLD signal, leaving the CNN with insufficient information to estimate RV accurately from BOLD signals alone. In these situations, head motion parameters can provide additional information that enhances the accuracy of the RV estimation.
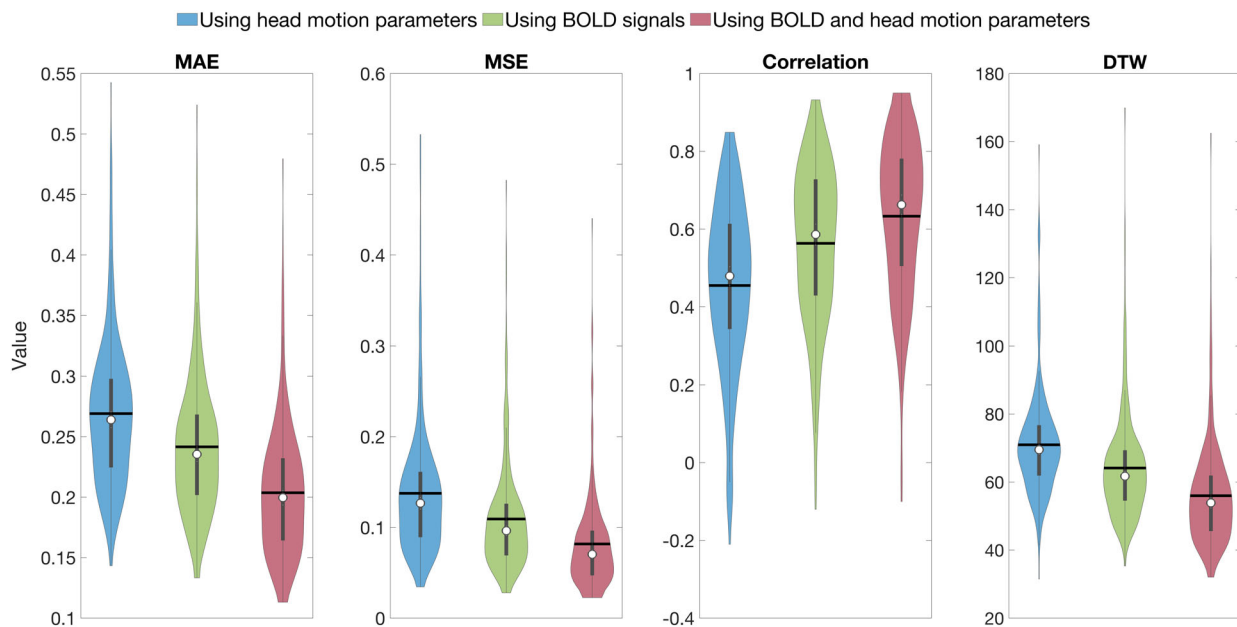

FIGURE 7 Violin plots comparing the performance metrics for RV reconstruction using three different approaches: Head motion parameters alone (blue), BOLD signals alone (green), and a combination of BOLD signals and head motion parameters (red). The metrics displayed are MAE, MSE, correlation coefficient, and DTW. The width of each violin represents the distribution of values across the dataset, with the white dot indicating the median, and a black horizontal line indicates the mean value. The combination of BOLD signals and head motion parameters (red) generally shows improved performance across all metrics, particularly in reducing MAE and MSE and increasing the correlation coefficient, compared to using BOLD signals or head motion parameters alone.

TABLE 1 Comparing the performance of the proposed method with Salas's model for all scans in the unseen test data in a 10-fold cross-validation.

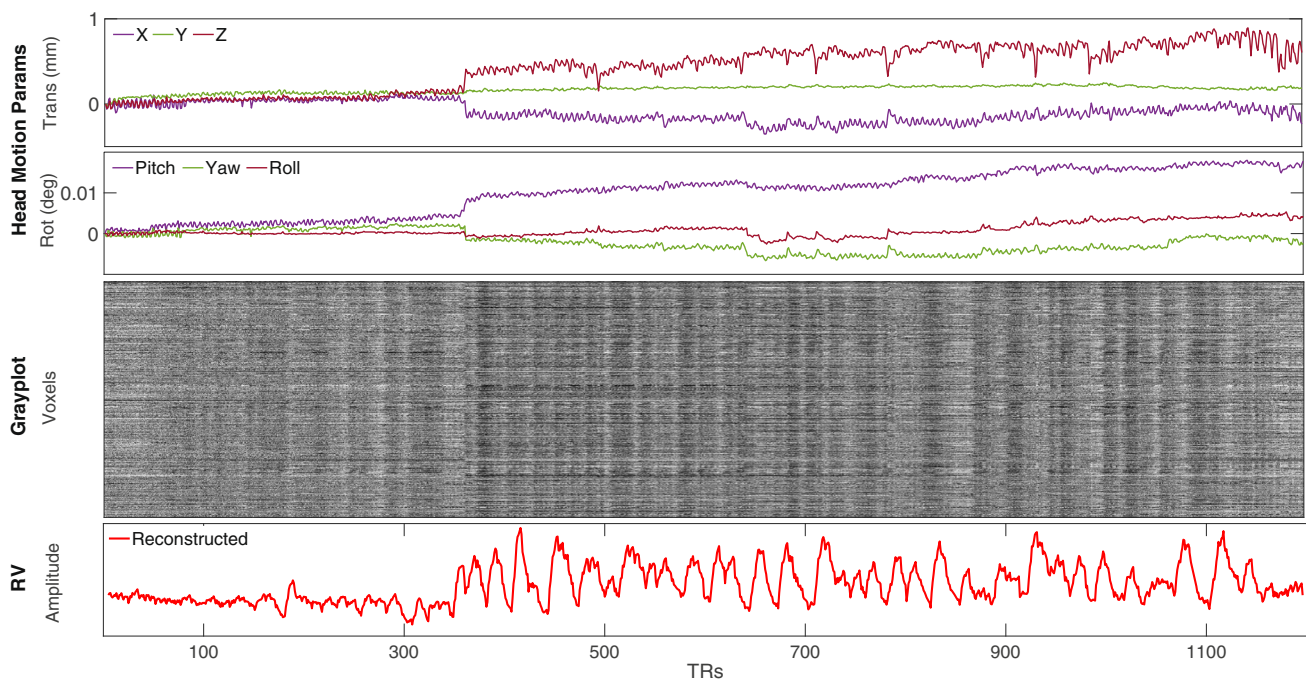| Method	Measure	MAE	MSE	r	DTW
Proposed method	Mean ± SE	0.204 ± 0.0026	0.082 ± 0.0057	0.64 ± 0.0076	55.26 ± 0.97
	Median ± SE	0.200 ± 0.0018	0.0705 ± 0.0030	0.67 ± 0.014	53.42 ± 0.62
Salas's model	Mean ± SE	0.225 ± 0.0014	0.102 ± 0.0083	0.59 ± 0.0091	61.52 ± 0.49
	Median ± SE	0.221 ± 0.0045	0.091 ± 0.0061	0.62 ± 0.035	58.01 ± 0.93

FIGURE 8 Reconstruction of the RV signal using the proposed method for an fMRI scan from the HCP-YA dataset where physiological data were not recorded (scan ID: 133019-REST 1-LR). Deep breaths are reflected as prominent bumps in the RV waveform, while the black vertical bands correspond to decreases in the BOLD signal following these deep breaths. The comparison of the estimated RV waveform with the grayplots and head motion parameters suggests a reliable estimation of respiratory fluctuations, even in the absence of direct physiological recordings.

3.3 | Evaluation of the proposed method on independent datasets

Dataset 1 consisted of 70 scans; however, due to partial corruption of respiratory data, only 41 scans were included in the final analysis. Dataset 2 comprised 461 scans, with 381 scans meeting the criteria for inclusion due to the availability of complete respiratory data (see Section 12 in Supporting Information). To ensure a meaningful comparison across these datasets, the HCP-YA dataset was resampled to match the TRs of Dataset 1 and Dataset 2. The CNN model was subsequently trained on the resampled HCP-YA data and tested on the two new datasets.

The results, summarized in Figure 9, underscore the effectiveness of the proposed method, which integrates both BOLD signals and head motion parameters. Figure 9A illustrates representative examples of reconstructed RV waveforms from both datasets, comparing the use of BOLD signals alone to the combined use of BOLD signals and head motion parameters. Figure 9B presents violin plots that further quantify the performance across multiple metrics.

In Dataset 1, the integration of head motion parameters led to significant reductions in MAE, MSE, and DTW, accompanied by an increase in correlation, thereby validating the efficacy of this combined approach. Statistical analysis confirmed a significant improvement ($p < 0.001$)
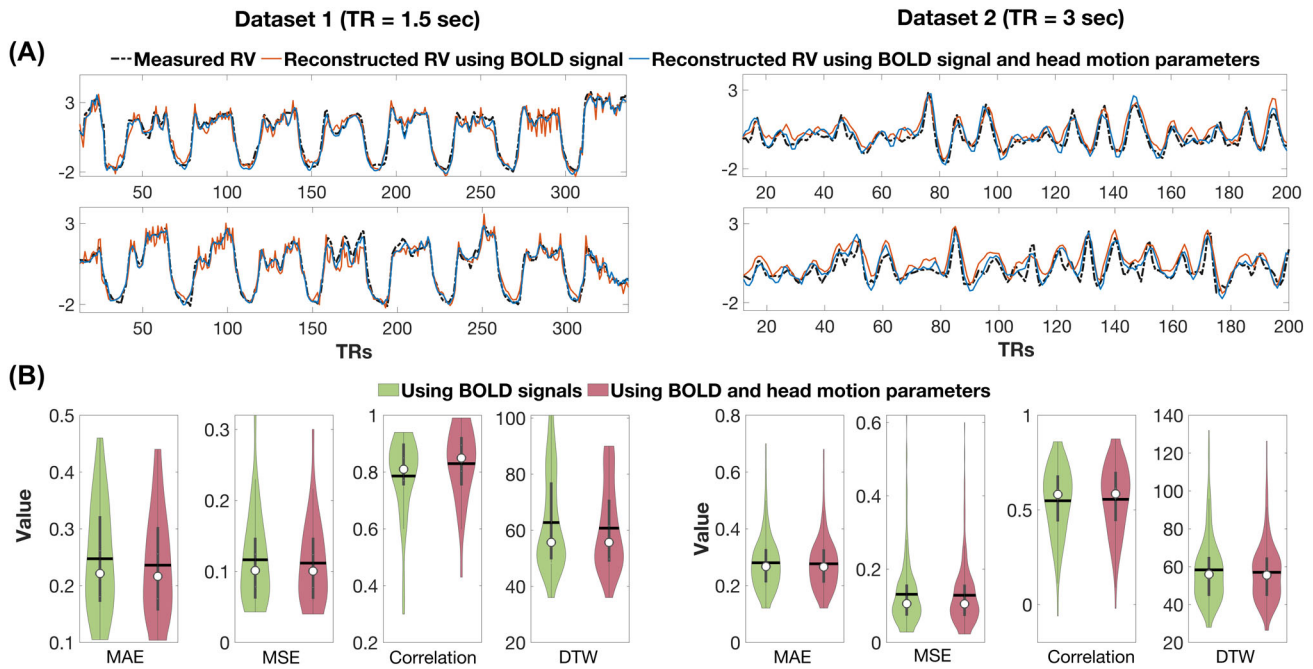
FIGURE 9 Reconstruction of respiratory variation (RV) using convolutional neural networks (CNNs) from BOLD-fMRI signals and head motion parameters across independent datasets. (A) Representative examples of reconstructed RV waveforms from two distinct datasets: Dataset 1 with a TR of 1.5 s, and Dataset 2 with a TR of 3 s. The comparison highlights the differences between RV waveforms reconstructed using BOLD signals alone and those reconstructed using both BOLD signals and head motion parameters. (B) Violin plots illustrate the performance metrics for RV reconstruction across the two datasets. Green violins represent reconstructions using only BOLD signals, while red violins indicate the inclusion of head motion parameters. The proposed method demonstrated significant improvements in Dataset 1, with the correlation coefficient increasing from $r = 0.78$ to $r = 0.83$, representing a 6.4% improvement, along with a reduction in error metrics, underscoring the effectiveness of integrating head motion parameters. In contrast, the performance on Dataset 2 was comparatively lower, likely due to the longer TR and associated aliasing effects, though the method still maintained a degree of robustness. This figure illustrates the method's generalizability and its variable efficacy depending on TR and dataset characteristics.

in models trained with both BOLD and head motion parameters compared to those trained with BOLD signals alone. This enhancement highlights the method's capacity to capture the intricate respiratory variations present in fMRI data, particularly in contexts with notable physiological fluctuations and shorter TRs.

Conversely, the results for Dataset 2 were more complex. Despite the inclusion of head motion parameters, the improvements were less pronounced, as indicated by a lower average correlation coefficient ($r = 0.55$) and elevated error metrics. This reduced performance is likely attributable to the aliasing effects associated with the longer TR, which complicate the extraction of relevant respiratory features. Although the method exhibited some degree of robustness in tracking RV, the improvements were not statistically significant ($p > 0.001$) when compared to using BOLD signals alone.

Overall, these findings affirm the generalizability of our proposed method across diverse experimental conditions. However, they also underscore the necessity for methodological adaptations to optimize the application of this approach across varying fMRI contexts.

4 | DISCUSSION

4.1 | Implications of respiratory variations in fMRI analysis

The method we present for reconstructing RV waveforms from BOLD-fMRI data enhances existing techniques by integrating head motion parameters to refine accuracy. This advancement is particularly relevant in functional neuroimaging, where the traditional reliance on external respiratory data often poses analytical challenges. By enhancing the precision of RV waveform extraction directly from fMRI data, our approach supports more accurate neural activation detection across diverse study populations, including those with irregular respiratory patterns and those intolerant to conventional monitoring devices.

The methodological enhancement carries significant logistical benefits. It promotes cost-efficiency and operational simplicity in fMRI studies by reducing the dependence on external respiratory monitoring equipment. Such a shift is beneficial across varied imaging settings, where equipment and expertise can differ markedly, as seen

in multi-site studies like the Adolescent Brain Cognitive Development study,[32] and the IMAGEN study.[33] By improving the standardization of respiratory data quality, the proposed approach ensures that all participants' data are subject to uniform analytical quality, irrespective of the site-specific variations in data collection protocols or technician expertise.

Enhancing the robustness of RV waveform reconstruction also has implications for increasing the statistical power of fMRI research. By enabling the use of previously unusable fMRI data affected by suboptimal respiratory records, our method can expand the volume of analyzable data, thus bolstering the statistical strength of studies. This is particularly valuable for large-scale datasets that lack comprehensive respiratory recordings, such as those from the Pediatric Imaging, Neurocognition, and Genetics study,[34] and the UK Biobank Brain Imaging project.[35] The potential for retrospective enhancement of these datasets demonstrates the added value of our refined approach.

Although the core methodology of reconstructing RV from fMRI data has been previously explored, the integration of head motion parameters significantly augments the precision and utility of this approach. The proposed refinement not only simplifies the data collection process but also enhances the overall quality and interpretability of neuroimaging data. Our contributions should be viewed as an evolutionary step in RV waveform reconstruction that addresses specific limitations of prior methods, thereby expanding their applicability and effectiveness in neuroimaging research.

4.2 | Incorporating head motion parameters

The primary differentiator in this study is the inclusion of head motion parameters to boost the accuracy of the machine learning algorithm. Previously, BOLD signals have been used for such estimations.[14–16] However, the realization that respiration-induced head movements can provide salient markers for respiratory events reshapes the paradigm. In the studies by Fair et al.[18] and Kaplan et al.,[19] a band-stop (also known as a notch) filter was employed to eliminate respiration-related effects from motion estimates. The results demonstrated that the use of such a filter enhances data quality and outcomes. These studies posited that respiration-related effects exist within certain frequency ranges, especially in the phase-encoding direction: [0.31, 0.43] Hz for the Adolescent Brain and Cognitive Development (ABCD) study, which involved participants aged 9–11,[18] and [0.25, 0.5] Hz for the Baby Connectome Project (BCP) with subjects averaging 14.3 ± 4.2 months old.[19] If respiratory effects have a designated frequency or

frequency range and can be eliminated using a band-stop filter, it suggests the filter suppresses this frequency range. Thus, it is conceivable that applying a bandpass filter centered on this range would isolate these respiratory-related components.

The visual differences in Figure 6 is subtle because it shows individual random examples from the 945 samples used in the study. These examples may not fully capture the variability or differences across the entire dataset. Figure 7, on the other hand, summarizes the performance across all samples, providing a more comprehensive view of the model differences. The quantitative metrics in Figure 7 reflect the overall trends and variability in model performance, which are not always apparent in a few individual examples.

In the aforementioned studies, the filter's bandwidth was chosen considering the entire cohort, making it notably broad. Excessively broad filters can diminish power in the overall trace. A static central frequency for the bandpass filter captures accurate respiratory-related motion only when it coincides with the actual breathing rate, leading to potential mismatches at other times. Such inconsistencies can mislead the machine learning model. Results from experiments detailed in the Supporting Information section, Table S.2 and Figure S.9 support these observations, demonstrating that use of bandpass filters significantly affects the model's ability to accurately reconstruct respiratory variations. We advise against using a fixed-frequency bandpass filter for isolating respiratory signals in machine-learning models. Instead, raw estimated head motion parameters should be used as they contain the full spectrum of motion-related information. Deep learning architectures, inherently capable of sophisticated nonlinear filtering, are better suited to discern and leverage patterns within the unprocessed data for RV reconstruction.

4.3 | Model performance and insights

The proposed technique is grounded in a set of assumptions. The interplay between breathing patterns, chemoreflexes, and head movements paves the way for RV estimation. Especially notable is the assertion that BOLD signals are influenced not just by immediate respiratory events but also by past breathing patterns, implying that the BOLD signal contains a memory of sorts of preceding respiratory events. This, when combined with the valuable data from head motion, can be tapped to gain a more comprehensive insight into RV. The model's commendable performance, as illustrated in the various figures, emphasizes the value of integrating multiple data streams. There are a few pertinent observations:

4.3.1 | Reconstructing high-variation RV

The CNN showcases heightened accuracy when reconstructing RV timeseries that have significant fluctuations. This suggests that, in scenarios where respiratory patterns are more dynamic, the model performs best. In contrast, it has challenges when the RV is constant.

4.3.2 | Significance of head motion parameters

The superior performance achieved when incorporating head motion parameters underlines their importance. The difference in accuracy when comparing both BOLD signals and head motion parameters versus using only BOLD signals is statistically significant. This elucidates the power of combining diverse data streams for comprehensive RV estimation.

However, for fMRI studies with larger TR, the aliasing of respiration-induced head motions into lower frequencies poses a significant challenge. This aliasing complicates the CNN's ability to effectively capture and utilize the full range of respiratory variations, particularly those occurring at higher frequencies. As a result, the convolutional neural network may struggle to extract and leverage the complete respiratory signal information, leading to potential reductions in the accuracy and robustness of the reconstructed respiratory variation waveforms. Nevertheless, with the increasing trend in fMRI studies utilizing higher field scanners and shorter TRs, our proposed method is well-suited to be effective in most current fMRI research. The method's design aligns with the prevailing practices in the field, ensuring its applicability and relevance across a broad range of modern fMRI studies.

4.3.3 | Impact of window size

The study underscores the profound effect of window size on the model's accuracy. Notably, as the window size expands, the distinction in performance between the two data input approaches (BOLD only vs. BOLD and motion parameters) diminishes, suggesting a diminishing return for larger windows. Use of a larger reconstruction time-window could potentially enable a broader range of RV frequencies to be captured by the model, though at the cost of increased complexity. Our method, which integrates the BOLD signal with head motion parameters, addresses the challenges of extensive window sizes and unnecessary complexity.

4.3.4 | Frequency content considerations

The analysis concerning PSD of RV provides intriguing insights. Specifically, when solely utilizing BOLD signals, the model grapples with capturing high-frequency components, an issue mitigated with the incorporation of head motion parameters.

4.4 | Limitations

While the current study yields promising results in reconstructing respiratory variations from resting state BOLD-fMRI data in healthy adult participants, we must acknowledge several limitations. First, the generalizability of the proposed method may be compromised by the homogeneous nature of the sample from HCP-YA. Despite the dataset's extensiveness, it does not feature individuals with respiratory conditions such as chronic obstructive pulmonary disease (COPD) or asthma, leaving the method's performance in a clinically diverse population untested.

Second, the method's efficacy across various age groups has not been examined. Relying solely on data from young adults ignores pediatric and older adult populations, which may have distinct respiratory rates and patterns due to age-related physiological changes.

Third, the focus of the current study on resting-state fMRI limits our ability to address the unique challenges associated with task-based fMRI. Task-based fMRI, which requires participants to perform specific cognitive or motor tasks during scans, involves complexities absent in resting-state studies.

Acknowledging these deficiencies, future research should incorporate datasets that represent a wider demographic, include individuals with respiratory diseases, span multiple age groups, account for varied scanning conditions, and incorporate task-based fMRI studies.

4.5 | Future work

The implications of our study extend to several prospective domains of research and technology, particularly within the realms of pediatric and geriatric neuroimaging. We envisage adapting our current methodology to better suit the intricate physiological profiles encountered in these age groups. This adaptation will involve the recalibration of our CNN to account for the distinctive variabilities in respiratory and neural patterns that manifest across the developmental and aging spectrums. Additionally, we will incorporate fMRI data with varied scan parameters to

improve the model's generalization and robustness across diverse experimental conditions.

Heart rate variability (HRV) has been established as a notable confounder in BOLD-fMRI analyses. Our subsequent efforts will be channeled toward the development of a robust computational model capable of discerning HRV directly from fMRI data. The realization of such a model aims to curtail the current reliance on peripheral monitoring technologies, thereby further streamlining the neuroimaging process.

Additional discussion can be found in the Supporting Information Sections 10 and 11, concerning the impact of hyperparameter tuning and addressing previous limitations.

5 | CONCLUSIONS

This study represents a substantial step forward in the domain of fMRI by enhancing the reconstruction of respiratory variations. The integration of BOLD signals and head motion parameters into a CNN has produced a model that surpasses previous attempts in accuracy. The improved performance, as evidenced by the reduction in MAE and MSE, along with increases in correlation and DTW, illustrates the untapped potential of machine learning techniques. The enhanced ability of the CNN to accurately reconstruct respiratory signals, even in the absence of direct respiratory data, opens the door to the retrospective examination of fMRI datasets and could significantly boost the quality of neuroimaging studies. Such advancements are crucial for progressing fMRI technologies and their application in both research and clinical settings, and they emphasize the critical role of integrating physiological data for the advancement of neuroimaging methodologies.

ORCID
M. Ethan MacDonald https://orcid.org/0000-0001-5421-3536

TWITTER
M. Ethan MacDonald MEthanMacDonald

REFERENCES
1. Birn RM, Diamond JB, Smith MA, Bandettini PA. Separating respiratory-variation-related fluctuations from neuronal-activity-related fluctuations in fMRI. *Neuroimage*. 2006;31:1536-1548.
2. Birn RM, Smith MA, Jones TB, Bandettini PA. The respiration response function: the temporal dynamics of fMRI signal fluctuations related to changes in respiration. *Neuroimage*. 2008;40:644-654. doi:10.1016/j.neuroimage.2007.11.059
3. Wise RG, Ide K, Poulin MJ, Tracey I. Resting fluctuations in arterial carbon dioxide induce significant low frequency variations in BOLD signal. *Neuroimage*. 2004;21:1652-1664.
4. Chang C, Cunningham JP, Glover GH. Influence of heart rate on the BOLD signal: the cardiac response function. *Neuroimage*. 2009;44:857-869.
5. Chang C, Glover GH. Relationship between respiration, end-tidal CO2, and BOLD signals in resting-state fMRI. *Neuroimage*. 2009;47:1381-1393.
6. Birn RM, Cornejo MD, Molloy EK, et al. The influence of physiological noise correction on test-retest reliability of resting-state functional connectivity. *Brain Connect*. 2014;4:511-522. doi:10.1089/brain.2014.0284
7. Chu PPW, Golestani AM, Kwinta JB, Khatamian YB, Chen JJ. Characterizing the modulation of resting-state fMRI metrics by baseline physiology. *Neuroimage*. 2018;173:72-87. doi:10.1016/j.neuroimage.2018.02.004
8. Golestani AM, Chen JJ. Controlling for the effect of arterial-CO2 fluctuations in resting-state fMRI: comparing end-tidal CO2 clamping and retroactive CO2 correction. *Neuroimage*. 2020;216:116874. doi:10.1016/j.neuroimage.2020.116874
9. Golestani AM, Kwinta JB, Strother SC, Khatamian YB, Chen JJ. The association between cerebrovascular reactivity and resting-state fMRI functional connectivity in healthy adults: the influence of basal carbon dioxide. *Neuroimage*. 2016;132:301-313. doi:10.1016/j.neuroimage.2016.02.051
10. Power JD, Lynch CJ, Dubin MJ, Silver BM, Martin A, Jones RM. Characteristics of respiratory measures in young adults scanned at rest, including systematic changes and "missed" deep breaths. *Neuroimage*. 2020;204:116234. doi:10.1016/j.neuroimage.2019.116234
11. Golestani AM, Chang C, Kwinta JB, Khatamian YB, Jean CJ. Mapping the end-tidal CO2 response function in the resting-state BOLD fMRI signal: spatial specificity, test–retest

reliability and effect of fMRI sampling rate. *Neuroimage.* 2015;104:266-277. doi:10.1016/j.neuroimage.2014.10.031

12. Addeh A, Vega F, Medi PR, Williams RJ, Pike GB, MacDonald ME. Direct machine learning reconstruction of respiratory variation waveforms from resting state fMRI data in a pediatric population. *Neuroimage.* 2023;269:119904. doi:10.1016/j.neuroimage.2023.119904

13. Power JD, Lynch CJ, Silver BM, Dubin MJ, Martin A, Jones RM. Distinctions among real and apparent respiratory motions in human fMRI data. *Neuroimage.* 2019;201:116041. doi:10.1016/j.neuroimage.2019.116041

14. Bayrak RG, Hansen CB, Salas JA, et al. From brain to body: learning low-frequency respiration and cardiac signals from fMRI dynamics. *From Brain to Body: Learning Low-Frequency Respiration and Cardiac Signals from fMRI Dynamics.* Springer International Publishing; 2021:553-563.

15. Bayrak RG, Salas JA, Huo Y, Chang C. *A Deep Pattern Recognition Approach for Inferring Respiratory Volume Fluctuations from fMRI Data.* Springer International Publishing; 2020:428-436.

16. Salas JA, Bayrak RG, Huo Y, Chang C. Reconstruction of respiratory variation signals from fMRI data. *Neuroimage.* 2021;225:117459. doi:10.1016/j.neuroimage.2020.117459

17. Chen JE, Glover GH. BOLD fractional contribution to resting-state functional connectivity above 0.1 Hz. *Neuroimage.* 2015;107:207-218. doi:10.1016/j.neuroimage.2014.12.012

18. Fair DA, Miranda-Dominguez O, Snyder AZ, et al. Correction of respiratory artifacts in MRI head motion estimates. *Neuroimage.* 2020;208:116400. doi:10.1016/j.neuroimage.2019.116400

19. Kaplan S, Meyer D, Miranda-Dominguez O, et al. Filtering respiratory motion artifact from resting state fMRI data in infant and toddler populations. *Neuroimage.* 2022;247:118838. doi:10.1016/j.neuroimage.2021.118838

20. Van de Moortele PF, Pfeuffer J, Glover GH, Ugurbil K, Hu X. Respiration-induced B0 fluctuations and their spatial distribution in the human brain at 7 tesla. *Magn Reson Med.* 2002;47:888-895. doi:10.1002/mrm.10145

21. Burgess GC, Kandala S, Nolan D, et al. Evaluation of denoising strategies to address motion-correlated artifacts in resting-state functional magnetic resonance imaging data from the human connectome project. *Brain Connect.* 2016;6:669-680.

22. Siegel JS, Mitra A, Laumann TO, et al. Data quality influences observed links between functional connectivity and behavior. *Cereb Cortex.* 2017;27:4492-4502.

23. Van Essen DC, Smith SM, Barch DM, et al. The WU-Minn human connectome project: an overview. *Neuroimage.* 2013;80:62-79.

24. Zvolanek KM, Moia S, Dean JN, Stickland RC, Caballero-Gaudes C, Bright MG. Comparing end-tidal CO2, respiration volume per time (RVT), and average gray matter signal for mapping cerebrovascular reactivity amplitude and delay with breath-hold task BOLD fMRI. *Neuroimage.* 2023;272:120038.

25. Spreng RN, Setton R, Alter U, et al. Neurocognitive aging data release with behavioral, structural and multi-echo functional MRI measures. *Sci Data.* 2022;9:119.

26. Van den Aardweg JG, Karemaker JM. Influence of chemoreflexes on respiratory variability in healthy subjects. *Am J Respir Crit Care Med.* 2002;165:1041-1047. doi:10.1164/ajrccm.165.8.2104100

27. Modarreszadeh M, Bruce EN. Ventilatory variability induced by spontaneous variations of PaCO2 in humans. *J Appl Physiol (1985).* 1994;76:2765-2775. doi:10.1152/jappl.1994.76.6.2765

28. Shirer WR, Ryali S, Rykhlevskaia E, Menon V, Greicius MD. Decoding subject-driven cognitive states with whole-brain connectivity patterns. *Cereb Cortex.* 2012;22:158-165. doi:10.1093/cercor/bhr099

29. Bishop CM, Nasrabadi NM. *Pattern Recognition and Machine Learning.* Vol 4. Springer; 2006.

30. Kuhn M, Johnson K. *Applied Predictive Modeling.* Springer; 2013.

31. Power JD. A simple but useful way to assess fMRI scan qualities. *Neuroimage.* 2017;154:150-158.

32. Casey BJ, Cannonier T, Conley MI, et al. The adolescent brain cognitive development (ABCD) study: imaging acquisition across 21 sites. *Dev Cogn Neurosci.* 2018;32:43-54. doi:10.1016/j.dcn.2018.03.001

33. Mascarell Maričić L, Walter H, Rosenthal A, et al. The IMAGEN study: a decade of imaging genetics in adolescents. *Mol Psychiatry.* 2020;25:2648-2671. doi:10.1038/s41380-020-0822-5

34. Jernigan TL, Brown TT, Hagler DJ, et al. The pediatric imaging, neurocognition, and genetics (PING) data repository. *Neuroimage.* 2016;124:1149-1154. doi:10.1016/j.neuroimage.2015.04.057

35. Miller KL, Alfaro-Almagro F, Bangerter NK, et al. Multimodal population brain imaging in the UK biobank prospective epidemiological study. *Nat Neurosci.* 2016;19:1523-1536. doi:10.1038/nn.4393

SUPPORTING INFORMATION

Additional supporting information may be found in the online version of the article at the publisher's website.

Data S1. Supporting Information.